

Correlating the end-Triassic mass extinction and flood basalt volcanism at the 100 ka level

Blair Schoene^{1*†}, Jean Guex^{2†}, Annachiara Bartolini^{3†}, Urs Schaltegger^{1†}, and Terrence J. Blackburn^{4†}

¹Earth Sciences, University of Geneva, Rue des Maraîchers 13, CH-1205 Geneva, Switzerland

²Geology and Paleontology, University of Lausanne, l'Anthropole, Lausanne, Switzerland

³Muséum National d'Histoire Naturelle, Histoire de la Terre, CP 38 CR2P UMR 7207 du CNRS, 8 rue Buffon, Paris, France

⁴Earth, Atmosphere and Planetary Sciences, Massachusetts Institute of Technology, 77 Massachusetts Avenue, Cambridge, Massachusetts 02142-1479, USA

ABSTRACT

New high-precision U/Pb geochronology from volcanic ashes shows that the Triassic-Jurassic boundary and end-Triassic biological crisis from two independent marine stratigraphic sections correlate with the onset of terrestrial flood volcanism in the Central Atlantic Magmatic Province to <150 ka. This narrows the correlation between volcanism and mass extinction by an order of magnitude for any such catastrophe in Earth history. We also show that a concomitant drop and rise in sea level and negative $\delta^{13}\text{C}$ spike in the very latest Triassic occurred locally in <290 ka. Such rapid sea-level fluctuations on a global scale require that global cooling and glaciation were closely associated with the end-Triassic extinction and potentially driven by Central Atlantic Magmatic Province volcanism.

INTRODUCTION

Mass extinctions reflect important interactions between biology, geology, geochemical cycles, and climate. The end-Triassic mass extinction is one of the five largest extinctions in Earth history, though considerable uncertainty remains in terms of its duration, causes, and effects. Many workers suggest that the extinction was related directly or indirectly to adverse climate following the onset of the Central Atlantic Magmatic Province (CAMP), which erupted $>2.5 \times 10^6 \text{ km}^3$ of basalt, possibly in $<1 \text{ Ma}$, making it perhaps the most voluminous flood basalt sequence of the Phanerozoic (Marzoli et al., 2004; McHone, 2003; Nomade et al., 2007; Whiteside et al., 2007). However, there remains a need for precise and accurate geochronology to correlate the onset of CAMP volcanism, recorded uniquely in terrestrial sections, with the well-documented marine extinction event (Marzoli et al., 2008; Tanner et al., 2004; Whiteside et al., 2007). Also lacking are time constraints for the rates of the Triassic-Jurassic boundary extinction and associated geochemical and paleoenvironmental fluctuations. We sampled three volcanic ash beds bracketing the Triassic-Jurassic boundary from the Pucara basin, northern Peru (Fig. 1A; Schaltegger et al., 2008), and also the first discovered ash bed from the New York Canyon, Nevada, which has been proposed as the Global Boundary and Stratotype Section and Point for the Triassic-Jurassic boundary (Guex et al., 2004). We also provide new U/Pb zircon data from two labs for the North

Mountain Basalt, the lowest CAMP basalt from the Fundy Basin, Nova Scotia (Greenough and Dostal, 1992). Both the ash beds and the North Mountain Basalt were dated using chemical abrasion–isotope dilution–thermal ionization mass spectrometry (CA-ID-TIMS; Mattinson, 2005) U-Pb zircon geochronology employing a new well-calibrated ^{202}Pb – ^{205}Pb – ^{233}U – ^{235}U tracer solution, which removes random uncertainty in mass fractionation during mass spectrometry. Data with this solution are as much as 70% more precise compared to single-Pb/single-U tracers, revealing complexity in tuff zircon populations that require new data interpretation strategies.

TRIASSIC-JURASSIC BOUNDARY

Recent consensus places the Triassic-Jurassic boundary at the first occurrence of the oldest Jurassic ammonite *Psiloceras spelae*, which marks the beginning of postextinction biodiversity recovery (Guex et al., 2004; Morton and Hesselbo, 2008). Pinpointing the extinction interval is more complicated, but coincides with a sharp negative spike in $\delta^{13}\text{C}$ at the end-Triassic, when there were steep declines in the biodiversity of ammonites, bivalves, radiolarians, corals, and conodonts (Morton and Hesselbo, 2008). This initial negative excursion is followed by a gradual positive recovery (Fig. 1B), which precedes a slow negative excursion in the Early Jurassic (beginning at bend N13 in Fig. 1B; Guex et al., 2004; Hesselbo et al., 2004; Kuerschner et al., 2007; Ward et al., 2001). The end-Triassic negative $\delta^{13}\text{C}$ excursion is recorded in marine organic and carbonate carbon and continent-derived wood material, illustrating that the anomaly resulted from a global carbon cycle perturbation (Galli et al., 2005; Hesselbo et al., 2004; Pálffy et al., 2001).

Proxies for rising atmospheric CO_2 have been reported from terrestrial fossil plants straddling the Triassic-Jurassic boundary (McElwain et al., 1999; Retallack, 2001), though the effects of other gases such as SO_2 on such proxies may also be important (Guex et al., 2004; Tanner et al., 2007). Terrestrial correlates to the marine extinction are debated (Lucas and Tanner, 2007; Tanner et al., 2004). An apparent palynological event $<1 \text{ m}$ below the lowest CAMP basalt in the Newark and Fundy Basins in North America was proposed as correlative of the Triassic-Jurassic boundary (Whiteside et al., 2007); this has been challenged on the basis of biostratigraphic and magnetostratigraphic work from North America and Morocco (Marzoli et al., 2004, 2008). Others argue that vertebrate and palynological biostratigraphy in the Newark and Fundy Basins, respectively, place the Triassic-Jurassic boundary in sedimentary slivers above the North Mountain Basalt (Lucas and Tanner, 2007; Cirilli et al., 2009).

An age for the marine Triassic-Jurassic boundary comes from the Pucara basin in northern Peru, where Schaltegger et al. (2008) reported a weighted-mean $^{206}\text{Pb}/^{238}\text{U}$ date of $201.58 \pm 0.18/0.38 \text{ Ma}$ (2σ ; without/with decay constant uncertainties). Abundant CAMP $^{40}\text{Ar}/^{39}\text{Ar}$ data cluster at 199 Ma (e.g., Nomade et al., 2007), but uncertainties of 1–2 Ma on individual dates in addition to the well-documented $\sim 0.7\%$ – 1% bias between the $^{40}\text{Ar}/^{39}\text{Ar}$ and U-Pb dating methods (Kuiper et al., 2008; Schoene et al., 2006) make this correlation imprecise. A $^{206}\text{Pb}/^{238}\text{U}$ date from the North Mountain Basalt of $201.27 \pm 0.06/0.30 \text{ Ma}$ (Schoene et al., 2006) would suggest that the CAMP postdates the Triassic-Jurassic boundary, precluding a causative relationship. However, those two U-Pb dates were measured using different tracer solutions, allowing for systematic bias and preventing high-precision comparison.

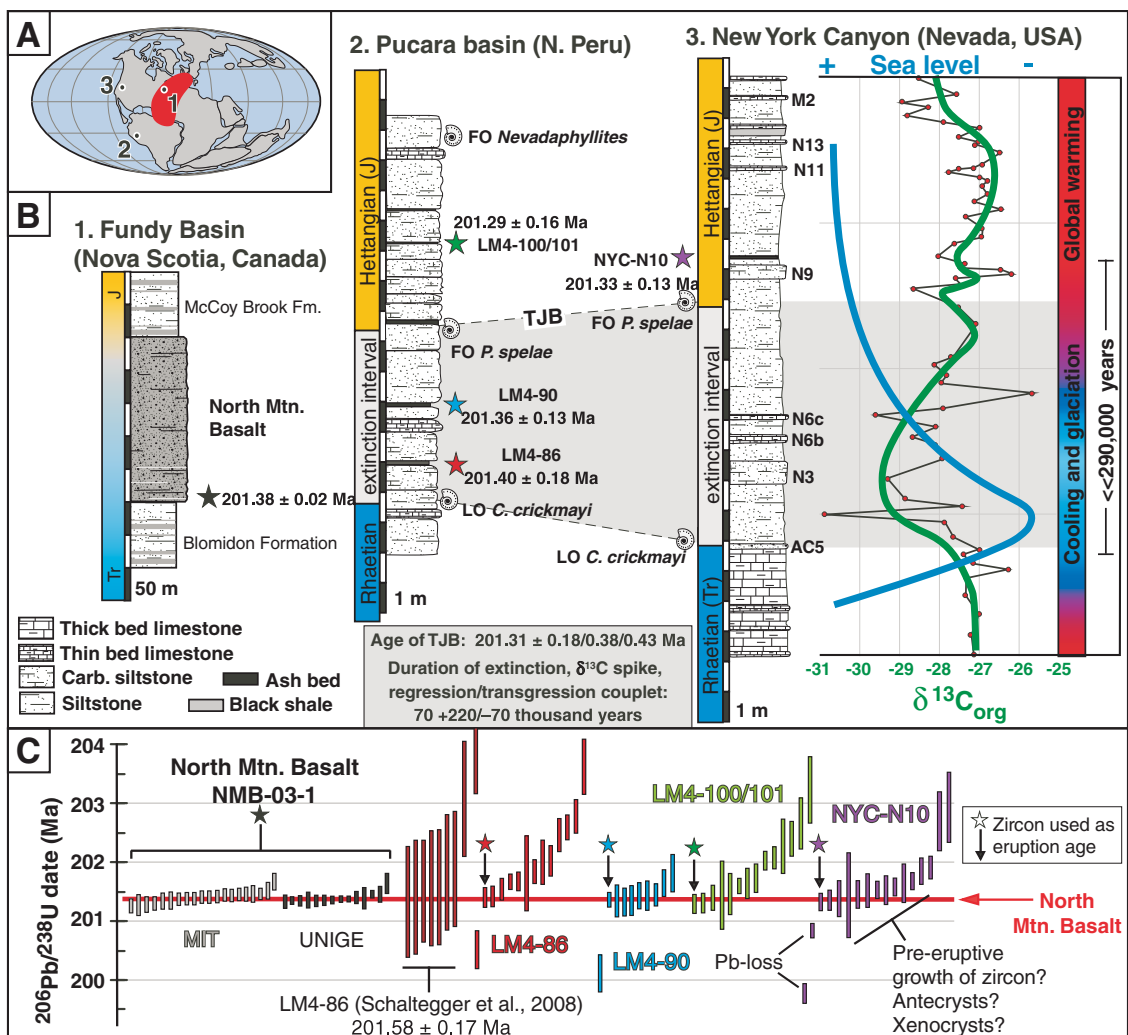
LOCALITIES AND U-Pb GEOCHRONOLOGY

We sampled three volcanic ash beds bracketing the Triassic-Jurassic boundary in the Pucara basin (samples LM4–86, LM4–90, and LM4–100/101; Figs. 1A, 1B), which is well calibrated biostratigraphically (Schaltegger et

*Current address: Geosciences, Guyot Hall, Princeton University, Princeton, New Jersey 08544, USA.

†E-mails: bschoene@princeton.edu; Jean.Guex@unil.ch; bartolini@mnhn.fr; urs.schaltegger@unige.ch; terrence@mit.edu.

Figure 1. A: Location map of three sections studied, with ca. 200 Ma paleogeography. Numbers correspond to stratigraphic sections in B. Red area outlines approximate extent of Central Atlantic Magmatic Province (e.g., McHone, 2003) B: Stratigraphic columns for sections studied; scale bars at bottom. J—Jurassic; Tr—Triassic. Fundy Basin section is after Whiteside et al. (2007). Pucara basin biostratigraphy is detailed in Schaltegger et al. (2008). New York Canyon stratigraphy, biostratigraphy, bed numbers, carbon isotopes, and sea-level curve are from Guex et al. (2004, 2008). Green curve in $\delta^{13}\text{C}$ plot is running mean of red data points. FO—first occurrence. LO—last occurrence; org—organic. Stars indicate ash beds sampled, with interpreted $^{206}\text{Pb}/^{238}\text{U}$ deposition age. All uncertainties are 2σ . TJB—Triassic-Jurassic boundary, defined as first occurrence of *Psiloceras spelae*. C: $^{206}\text{Pb}/^{238}\text{U}$ dates for single-grain zircons, color-coded to sample locations in B. Date for LM4-86 from Schaltegger et al. (2008) includes tracer calibration uncertainty. Data for North Mountain Basalt are from Massachusetts Institute of Technology (MIT) and University of Geneva (UNIGE); all ash-bed data are from University of Geneva.



al., 2008). In this section, the disappearance of the latest Triassic ammonite *Choristoceras crickmayi* immediately precedes the peak extinction rate (Guex et al., 2004). One ash bed sample (NYC-N10) was collected ~1.5 m above the first occurrence of *P. spelae* in the New York Canyon section, for which detailed $\delta^{13}\text{C}$ and biostratigraphic data have been published (Guex et al., 2004, 2008) (Figs. 1A, 1B). We also provide new U/Pb data from two laboratories for the North Mountain Basalt (NMB-03-1). All dates were produced using CA-ID-TIMS on single zircons relative to the new EARTHTIME (<http://www.earth-time.org/>) ($\pm^{202}\text{Pb}$), ^{205}Pb - ^{233}U - ^{235}U tracer solution, allowing us to ignore tracer calibration uncertainties within this study (Schoene et al., 2006). All uncertainties are reported at the 2σ level, have been corrected for ^{230}Th disequilibrium, and omit decay constant uncertainties unless otherwise noted (see the GSA Data Repository¹ for analytical details). $^{206}\text{Pb}/^{238}\text{U}$ dates for single zircons are plotted in Figure 1C and concor-

dia plots and U-Pb data are presented in Figure DR1 and Table DR1, respectively.

Ash beds yielded 20–100 zircons between 50 and 200 μm in diameter (see the Data Repository); 14 zircons from sample LM4-86 give $^{206}\text{Pb}/^{238}\text{U}$ dates that span ~1.5 Ma between 201 and 203 Ma, with one older and one younger grain. The main population is not statistically equivalent, with a high mean square of weighted deviates (MSWD) of 12 on a weighted-mean $^{206}\text{Pb}/^{238}\text{U}$ date (i.e., many dates do not overlap at 2σ). Similarly, LM4-90 and LM4-100/101 yield zircon populations that spread between 0.4 and >1 Ma with high MSWD values. LM4-90 also has one grain ca. 200.1 Ma and a population of ca. 900 Ma xenocrystic zircons. Of 17 zircons from NYC-N10, 15 give $^{206}\text{Pb}/^{238}\text{U}$ dates

¹GSA Data Repository item 2010109, U-Pb data table, analytical details, and additional figures, is available online at www.geosociety.org/pubs/ft2010.htm, or on request from editing@geosociety.org or Documents Secretary, GSA, P.O. Box 9140, Boulder, CO 80301, USA.

between 201.3 and 201.9 Ma; a weighted-mean yields an MSWD of >2. Two younger grains give $^{206}\text{Pb}/^{238}\text{U}$ dates younger than 201 Ma and two older grains of ca. 203 Ma (Fig. 1C).

Analyses of 13 single grains of the North Mountain Basalt (NMB-03-1) from the University of Geneva and 19 analyses from the Massachusetts Institute of Technology are statistically equivalent, yielding a weighted-mean $^{206}\text{Pb}/^{238}\text{U}$ date of $201.38 \pm 0.02/0.22/0.31$ Ma (internal uncertainties/with tracer calibration uncertainties/with decay constant uncertainties; omitting two analyses, MSWD = 1.2).

INTERPRETING DEPOSITION AGES FOR ASH BEDS

U/Pb ages for volcanic ash beds are often determined by calculating a weighted-mean date and thus assuming that there exists a single population of zircons that crystallized immediately prior to eruption (Ramezani et al., 2007; Schaltegger et al., 2008). Our ash-bed data reveal complicated U-Pb systematics, precluding such

an interpretation. The observed spread in dates could be created by several effects: (1) analytical bias and underestimated uncertainties, (2) postcrystallization loss of radiogenic Pb from zircons, or (3) zircons representing a range of growth histories prior to eruption. The equivalency of the North Mountain Basalt data from two independent laboratories using a single tracer solution, transparent data-reduction techniques (Schmitz and Schoene, 2007), and careful analytical blank calibration (see the Data Repository) suggests that tuff zircon data are equally accurate and analytical uncertainties are correctly estimated.

Despite the overall success of the chemical abrasion technique at removing the effects of Pb loss (Mattinson, 2005), three of four ash-bed samples have at least one zircon that is far younger than the main population, and we suggest that these outliers are the result of residual Pb loss. There is a simple test suggesting that the main population of zircons did not also undergo Pb loss: the youngest zircon from the main population of each sample is younger or within uncertainty than that of the sample stratigraphically below it. This would be remarkably coincidental if these populations had undergone Pb loss.

We interpret the spread in $^{206}\text{Pb}/^{238}\text{U}$ dates of the main population of tuff zircons to be the result of protracted growth of zircon in the magmatic system and/or the incorporation of xenocrystic zircon. Complex volcanic and plutonic systems involving small magma batches, mafic and silicic replenishment, magma mingling and/or mixing, and crustal assimilation can entrain antecrystic to xenocrystic zircons with dates recording millions of years of magmatic activity (Charlier et al., 2005; Crowley et al., 2007; Simon and Reid, 2005; Miller et al., 2007). Th/U ratios of zircons from each of our ash samples plot into distinct but overlapping groups (Fig. DR2). This argues that younger ashes came from a different magma batch, but may have incorporated reworked ash material and/or xenocrystic zircons. Zircon morphology supports this: the youngest grains had the highest aspect ratios and were prismatic and euhedral (typical of rhyolitic zircon), whereas older populations contained similarly euhedral grains in addition to anhedral rounded grains. Thus, although zircon selection is critical in avoiding xenocrysts, the increased precision afforded by the ^{202}Pb - ^{205}Pb - ^{233}U - ^{235}U tracer can also identify euhedral zircons that predate eruption. The zircons from LM4-86 dated (Schaltegger et al., 2008) with a ^{205}Pb - ^{235}U tracer likely record the same population of zircons as this study, though it appeared as one population due to increased uncertainties on single analyses (Fig. 1C). Such an observation demands caution when taking weighted means of large populations, especially in lower precision data sets.

Therefore, we use the youngest single closed-system zircon to approximate the eruption date (Figs. 1B, 1C). A less conservative interpretation uses weighted means of several zircons, with the resulting MSWD as a guide. Those eruption ages overlap with the single-grain interpretation and with the age of the North Mountain Basalt (Table DR3).

TIMING AND RATES OF EVENTS AT THE TRIASSIC-JURASSIC BOUNDARY

A $^{206}\text{Pb}/^{238}\text{U}$ age of the Triassic-Jurassic boundary in the Pucara basin, defined as the first appearance of *P. spelae*, can be calculated using our new data to be $201.31 \pm 0.18/0.38/0.43$ Ma, using the difference between the minimum age of LM4-100/101 and the maximum age of LM4-90. This correlates to the onset of the CAMP in the Fundy Basin to within ± 150 ka (Fig. 1B).

Our data also provide tie points between the terrestrial Triassic-Jurassic boundary, located near the North Mountain Basalt (Cirilli et al., 2009), and the marine ammonite extinction in two stratigraphic sections. The deposition age from NYC-N10 in Nevada is identical to that from LM4-100/101 in Peru, illustrating that the first appearance of *P. spelae* in both sections is contemporaneous within our resolution. If we assume that the last occurrence of *C. crickmayi* in the New York Canyon is also correlative with that in the Pucara basin, we can conclude that the duration of the end-Triassic negative $\delta^{13}\text{C}_{\text{organic}}$ excursion was $70 \pm 220/-70$ ka (the duration between LM4-86 and NYC-N10), which also serves as an estimate for the duration of the mass extinction event.

DISCUSSION

Some numerical carbon cycle models suggest that CO_2 released from flood basalts is insufficient to create the end-Triassic negative $\delta^{13}\text{C}$ anomaly and that associated with the Permian-Triassic extinction (Beerling and Berner, 2002; Payne and Kump, 2007). Alternatively, it is hypothesized that CAMP volcanism may have destabilized methane hydrates or accessed large carbon reservoirs by erupting through organic-rich sediment, resulting in massive input of light carbon into the oceans and atmosphere, creating a <200 ka negative $\delta^{13}\text{C}$ spike (Beerling and Berner, 2002; Pálffy et al., 2001; Retallack, 2001), which is consistent with our geochronological data. However, recent work suggests that SO_2 and polycyclic aromatic hydrocarbons were drivers in rapid and widespread terrestrial plant turnover, rather than CO_2 and greenhouse warming (Van de Schootbrugge et al., 2009). Furthermore, Korte et al. (2009) provided $\delta^{18}\text{O}$ data from fossil oysters that argue for cool ocean temperatures immediately after the initial negative $\delta^{13}\text{C}$ excursion (after the extinction event in the New York Canyon), followed by $\sim 8^\circ\text{C}$ early

Hettangian warming. These recent studies argue that CO_2 -induced global warming was not the driver for the end-Triassic biotic crisis, but allow that it was important in the postextinction recovery interval.

The short duration (<290 ka) for the marine regression-transgression sequence in the New York Canyon provided by our geochronological data gives an additional constraint. Latest Triassic regression-transgression is recognized in numerous sections in Europe and North America, and is likely the result of global sea-level change (Hallam and Wignall, 1999). Several sections in Europe also show it coupled to the Late Triassic negative $\delta^{13}\text{C}$ excursion, as seen in the New York Canyon (Fig. 1B) (e.g., Galli et al., 2005; Hesselbo et al., 2004; Kuerschner et al., 2007). Global eustasy results from a variety of processes, including continental uplift due to thermal underplating (e.g., by a plume) or changes in volumes or rates of mid-ocean ridge production, but these processes occur on time scales longer than 1 Ma (e.g., Miller et al., 2005). The rapid sea-level fluctuation we document for the latest Triassic can only be explained by glacial eustasy. A model that accounts for this observation was proposed in Guex et al. (2004), and suggested that the negative $\delta^{13}\text{C}$ excursion in the uppermost Triassic (Fig. 1B) was associated with extinction and primary productivity collapse caused by volcanic SO_2 and heavy metals emissions, acid rain, and a cooling and glacial event that caused a short but major drop in sea level. This first phase was followed by CAMP-related CO_2 accumulation, greenhouse warming, marine transgression, and postextinction biotic recovery, corresponding to the positive and second negative $\delta^{13}\text{C}$ excursions (Fig. 1B).

Fingerprinting the trigger for the end-Triassic ecological disaster must come from additional biological and environmental proxy data in combination with high-precision geochronology in other Triassic-Jurassic boundary sections. Such work will better constrain the rates of CAMP eruption and corroborate that sea-level change and extinction were everywhere fast and contemporaneous (Hallam and Wignall, 1999; Hesselbo et al., 2004). Our new U-Pb data show that such constraints can be facilitated using new freely available EARTHTIME ($\pm^{202}\text{Pb}$)- ^{205}Pb - ^{233}U - ^{235}U tracers, by effectively eliminating interlaboratory bias and substantially increasing both internal and external precision of U-Pb ID-TIMS dating.

ACKNOWLEDGMENTS

Guex, Schaltegger, and Schoene were supported by the Suisse Fonds National, and Guex acknowledges stimulating discussions with D. Taylor. We thank J. Ramezani for assistance with the North Mountain Basalt dating at the Massachusetts Institute of Technology (MIT). Helpful suggestions from A. Marzoli and two other reviewers improved this paper. Support at MIT comes from National Science Foundation grant EAR-0446880 and the EARTHTIME initiative.

REFERENCES CITED

- Beerling, D.J., and Berner, R.A., 2002, Biogeochemical constraints on the Triassic-Jurassic boundary carbon cycle event: *Global Biogeochemical Cycles*, v. 16, 1036, doi: 10.1029/2001GB001637.
- Charlier, B.L.A., Wilson, C.J.N., Lowenstern, J.B., Blake, S., Van Calstren, P.W., and Davidson, J.P., 2005, Magma generation at a large hyperactive silicic volcano (Taupo, New Zealand) revealed by U-Th and U-Pb systematics in zircons: *Journal of Petrology*, v. 46, p. 3–32, doi: 10.1093/ptrology/egh060.
- Cirilli, S., Marzoli, A., Tanner, L., Bertrand, H., Buratti, N., Jourdan, F., Bellieni, G., Kontak, D., and Renne, P.R., 2009, Latest Triassic onset of the Central Atlantic Magmatic Province (CAMP) volcanism in the Fundy Basin (Nova Scotia): New stratigraphic constraints: *Earth and Planetary Science Letters*, v. 286, p. 514–525, doi: 10.1016/j.epsl.2009.07.021.
- Crowley, J.L., Schoene, B., and Bowring, S.A., 2007, U-Pb dating of zircon in the Bishop Tuff at the millennial scale: *Geology*, v. 35, p. 1123–1126, doi: 10.1130/G24017A.1.
- Galli, M.T., Jadoul, F., Bernasconi, S.M., and Weisert, H., 2005, Anomalies in global carbon cycling and extinction at the Triassic/Jurassic boundary: Evidence from a marine C-isotope record: *Palaeogeography, Palaeoclimatology, Palaeoecology*, v. 216, p. 203–214, doi: 10.1016/j.palaeo.2004.11.009.
- Greenough, J.D., and Dostal, J., 1992, Cooling history and differentiation of a thick North Mountain Basalt flow (Nova Scotia, Canada): *Bulletin of Volcanology*, v. 55, p. 63–73, doi: 10.1007/BF00301120.
- Guex, J., Bartolini, A., Atudorei, V., and Taylor, D., 2004, High-resolution ammonite and carbon isotope stratigraphy across the Triassic-Jurassic boundary at New York Canyon (Nevada): *Earth and Planetary Science Letters*, v. 225, p. 29–41, doi: 10.1016/j.epsl.2004.06.006.
- Guex, J., Bartolini, A., Taylor, D., Atudorei, V., Thelin, P., Bruchez, S., Tanner, L.H., and Lucas, S.G., 2008, The organic carbon isotopic and paleontological record across the Triassic-Jurassic boundary at the candidate GSSP section at Ferguson Hill, Muller Canyon, Nevada, USA: Comment: *Palaeogeography, Palaeoclimatology, Palaeoecology*, v. 273, p. 205–206.
- Hallam, A., and Wignall, P.B., 1999, Mass extinctions and sea-level changes: *Earth-Science Reviews*, v. 48, p. 217–250, doi: 10.1016/S0012-8252(99)00055-0.
- Hesselbo, S.P., Robinson, S.A., and Surlyk, F., 2004, Sea-level change and facies development across potential Triassic-Jurassic boundary horizons, SW Britain: *Geological Society of London Journal*, v. 161, p. 365–379.
- Korte, C., Hesselbo, S.P., Jenkyns, H.C., Rickaby, R.E.M., and Spöli, C., 2009, Palaeoenvironmental significance of carbon- and oxygen-isotope stratigraphy of marine Triassic Jurassic boundary sections in SW Britain: *Geological Society of London Journal*, v. 166, p. 431–445, doi: 10.1144/0016-76492007-177.
- Kuerschner, W.M., Bonis, N.R., and Krystyn, L., 2007, Carbon-isotope stratigraphy and palynostratigraphy of the Triassic-Jurassic transition in the Tiefengraben section—Northern Calcareous Alps (Austria): *Palaeogeography, Palaeoclimatology, Palaeoecology*, v. 244, p. 257–280, doi: 10.1016/j.palaeo.2006.06.031.
- Kuiper, K.F., and Deino, A., Hilgen, F.J., Krijgsman, W., Renne, P.R., and Wijbrans, J.R., 2008, Synchronizing rocks clocks of Earth history: *Science*, v. 320, p. 500–504.
- Lucas, S.G., and Tanner, L.H., 2007, The non-marine Triassic-Jurassic boundary in the Newark Supergroup of eastern North America: *Earth-Science Reviews*, v. 84, p. 1–20, doi: 10.1016/j.earscirev.2007.05.002.
- Marzoli, A., and 14 others, 2004, Synchrony of the Central Atlantic magmatic province and the Triassic-Jurassic boundary climatic and biotic crisis: *Geology*, v. 32, p. 973–976, doi: 10.1130/G20652.1.
- Marzoli, A., Bertrand, H., Knight, K.B., Cirilli, S., Nomade, S., Renne, P.R., Verati, C., Youbi, N., Martini, R., and Bellieni, G., 2008, Synchrony between the Central Atlantic magmatic province and the Triassic-Jurassic mass-extinction event?: Comment: *Palaeogeography, Palaeoclimatology, Palaeoecology*, v. 262, p. 189–193, doi: 10.1016/j.palaeo.2008.01.016.
- Mattinson, J.M., 2005, Zircon U-Pb chemical-abrasion (“CA-TIMS”) method: Combined annealing and multi-step dissolution analysis for improved precision and accuracy of zircon ages: *Chemical Geology*, v. 220, p. 47–56, doi: 10.1016/j.chemgeo.2005.03.011.
- McElwain, J.C., Beerling, D.J., and Woodward, F.I., 1999, Fossil plants and global warming at the Triassic-Jurassic Boundary: *Science*, v. 285, p. 1386–1390, doi: 10.1126/science.285.5432.1386.
- McHone, J.G., 2003, Volatile emissions from Central Atlantic Magmatic Province basalts; mass assumptions and environmental consequences, *in* Hames, W.E., et al., eds., *The Central Atlantic Magmatic Province; insights from fragments of Pangea: American Geophysical Union Geophysical Monograph* 136, p. 241–254.
- Miller, J.S., Matzel, J.P., Miller, C.F., Burgess, S.D., and Miller, R.B., 2007, Zircon growth and recycling during the assembly of large, composite arc plutons: *Journal of Volcanology and Geothermal Research*, v. 167, p. 282–299, doi: 10.1016/j.jvolgeores.2007.04.019.
- Miller, K.G., Komins, M.A., Browning, J.V., Wright, J.D., Mountain, G.S., Katz, M.E., Sugarman, P.J., Carter, B.S., Christie-Blick, N., and Pekar, S.F., 2005, The Phanerozoic record of global sea-level change: *Science*, v. 310, p. 1293–1298, doi: 10.1126/science.1116412.
- Morton, N., and Hesselbo, S., eds., 2008, Details of voting on proposed GSSP and ASSP for the base of the Hettangian Stage and Jurassic System: *International Subcommittee on Jurassic Stratigraphy Newsletter*, v. 35, part 1, December, 76 p.
- Nomade, S., Knight, K.B., Beutel, E., Renne, P.R., Verati, C., Féraud, G., Marzoli, A., Youbi, N., and Bertrand, H., 2007, Chronology of the Central Atlantic Magmatic Province: Implications for the Central Atlantic rifting processes and the Triassic-Jurassic biotic crisis: *Palaeogeography, Palaeoclimatology, Palaeoecology*, v. 244, p. 326–344, doi: 10.1016/j.palaeo.2006.06.034.
- Pálffy, J., Demény, A., Haas, J., Hetényi, M., Orchard, M.J., and Vető, I., 2001, Carbon isotope anomaly and other geochemical changes at the Triassic-Jurassic boundary from a marine section in Hungary: *Geology*, v. 29, p. 1047–1050, doi: 10.1130/0091-7613(2001)029<1047:CIAAOG>2.0.CO;2.
- Payne, J.L., and Kump, L.R., 2007, Evidence for recurrent Early Triassic massive volcanism from quantitative interpretation of carbon isotope fluctuations: *Earth and Planetary Science Letters*, v. 256, p. 264–277, doi: 10.1016/j.epsl.2007.01.034.
- Ramezani, J., Schmitz, M.D., Davydov, V.I., Bowring, S.A., Snyder, W.S., and Northrup, C.J., 2007, High-precision U-Pb zircon age constraints on the Carboniferous-Permian boundary in the southern Urals stratotype: *Earth and Planetary Science Letters*, v. 256, p. 244–257, doi: 10.1016/j.epsl.2007.01.032.
- Retallack, G.J., 2001, A 300-million year record of atmospheric carbon dioxide from fossil plant cuticles: *Nature*, v. 411, p. 287–290, doi: 10.1038/35077041.
- Schaltegger, U., Guex, J., Bartolini, A., Schoene, B., and Ovtcharova, M., 2008, Precise U-Pb age constraints for end-Triassic mass extinction, its correlation to volcanism and Hettangian post-extinction recovery: *Earth and Planetary Science Letters*, v. 267, p. 266–275, doi: 10.1016/j.epsl.2007.11.031.
- Schmitz, M.D., and Schoene, B., 2007, Derivation of isotope ratios, errors, and error correlations for U-Pb geochronology using 205Pb-235U-(233U)-spike isotope dilution thermal ionization mass spectrometric data: *Geochemistry Geophysics Geosystems*, v. 8, Q08006, doi: 10.1029/2006GC001492.
- Schoene, B., Crowley, J.L., Condon, D.C., Schmitz, M.D., and Bowring, S.A., 2006, Reassessing the uranium decay constants for geochronology using ID-TIMS U-Pb data: *Geochimica et Cosmochimica Acta*, v. 70, p. 426–445, doi: 10.1016/j.gca.2005.09.007.
- Simon, J.I., and Reid, M.R., 2005, The pace of rhyolite differentiation and storage in an ‘archetypical’ silicic magma system, Long Valley, California: *Earth and Planetary Science Letters*, v. 235, p. 123–140, doi: 10.1016/j.epsl.2005.03.013.
- Tanner, L.H., Lucas, S.G., and Chapman, M.G., 2004, Assessing the record and causes of Late Triassic extinctions: *Earth-Science Reviews*, v. 65, p. 103–139, doi: 10.1016/S0012-8252(03)00082-5.
- Tanner, L., Smith, D.L., and Allan, A., 2007, Stomatal response of swordfern to volcanogenic CO₂ and SO₂ from Kilauaea volcano: *Geophysical Research Letters*, v. 34, L15807, doi: 10.1029/2007GL030320.
- Van de Schootbrugge, B., Quan, T.M., Lindström, S., Püttmann, W., Heunisch, C., Pross, J., Fiebig, J., Petschick, R., Röhling, H.-G., Rigoz, S., Rosenthal, Y., and Falkowski, P.G., 2009, Floral changes across the Triassic/Jurassic boundary linked to flood basalt volcanism: *Nature Geoscience*, v. 2, p. 589–594, doi: 10.1038/ngeo577.
- Ward, P.D., Haggart, J.W., Carter, E.S., Wilbur, D., Tipper, H.W., and Evans, T., 2001, Sudden productivity collapse associated with the Triassic-Jurassic boundary mass extinction: *Science*, v. 292, p. 1148–1151, doi: 10.1126/science.1058574.
- Whiteside, J.H., Olsen, P.E., Kent, D.V., Fowell, S.J., and Et-Touhami, M., 2007, Synchrony between the Central Atlantic magmatic province and the Triassic-Jurassic mass-extinction event?: *Palaeogeography, Palaeoclimatology, Palaeoecology*, v. 244, p. 345–367, doi: 10.1016/j.palaeo.2006.06.035.

Manuscript received 11 September 2009

Revised manuscript received 13 November 2009

Manuscript accepted 13 November 2009

Printed in USA

SUPPLEMENTARY ONLINE MATERIAL

Sample descriptions and analytical methods. NMB-03-1, the North Mtn. Basalt, was collected at the location described in Schoene et al. (2006) and Hodych and Dunning (1992). It comes from pegmatitic segregations within the lowest basaltic flow, which were interpreted by Greenough and Dostal (1992) to have formed *in situ* after eruption of the basalt, and therefore zircon dates from these segregations very closely date the eruption (further description of the NMB is found in Kontak; 2008). Our sample was processed at MIT using standard crushing and mineral separation procedure. It yielded abundant stubby prismatic grains from which single grains were selected for chemical abrasion. Ash sample NYC-N10 was taken from the New York canyon section, Nevada, USA, whose location is described in Guex et al. (2004) and Ward et al. (2007). The GPS location for *P. spelae* in this section is N 38°29'10.6", W 118°05'0.72". The other ash samples come from the Pucara Group sediments in the Utcubamba Valley, Northern Peru, which is described in Schaltegger et al. (2008). The GPS location for *P. spelae* in this section is S 06°18'28.5", W 77°53'16.2". Sampled ash beds were between 1 and 7 cm thick and consisted of gray to green to yellow fine-grained material. Ashes were processed at UNIGE by first crushing with a hammer in a plastic bag and then placed in a tungsten mill shatterbox for five second increments and sieved to <500 µm. Separated material was then washed with water in a large beaker and decanted multiple times to remove clay material, and the resulting separates were put through magnetic and heavy liquid separation. This resulted in between 100 (LM4-100/101) and 20 zircons (NYC-N10). Single grains were picked for chemical abrasion and combined in a quartz beaker

for annealing at 900 °C for ~60 hours. All grains from a single sample were leached together in 3 ml savillex beakers in HF + trace HNO₃ for ~12 hours, rinsed with water and acetone and then placed in 6N HCl on a hotplate at ~110 °C overnight. These were then washed several times with water, HCl, and HNO₃. Single grains were then handpicked for dissolution, which varied from short and stubby to long and prismatic with variable levels of clarity. There was no obvious correlation between grain morphology and age in any of the analyzed samples, though youngest ash zircons were always long and prismatic. Each grain was spiked with ~0.004 g of the EARTHTIME ($\pm^{202}\text{Pb}$)- ^{205}Pb - ^{233}U - ^{235}U tracer solution. Zircons were dissolved in ~70 μl 40% HF and trace HNO₃ in 200 μl savillex capsules at 210 °C for 48+ hours, dried down and redissolved in 6N HCl overnight. Samples were then dried down and redissolved in 3N HCl and put through a modified single 50 μl column anion exchange chemistry (Krogh, 1973). U and Pb were collected in the same beaker and dried down with a drop of 0.05 M H₃PO₄, and analyzed on a single outgassed Re filament in a Si-gel emitter, modified from Gerstenberger and Haas (Gerstenberger and Haase, 1997). Measurements were performed on a Thermo-Finigan Triton thermal ionization mass spectrometer at UNIGE and a VG S54 thermal ionization mass spectrometer at MIT.

On the Triton, Pb was measured in dynamic mode on a modified Masscom secondary electron multiplier (SEM). Deadtime for the SEM was determined by periodic measurement of NBS-982 for up to 1.3 Mcps and observed to be constant at 23.5 ns. Multiplier linearity was monitored every few days between 1.3×10^6 and <100 cps by a combination of measurements of NBS-981, -982 and -983, and observed to be constant if the Faraday to SEM yield was kept between ~93-94% by adjusting SEM voltage.

Baseline measurements were made at masses 203.5 and 204.5 and the average was subtracted from each peak after beam decay correction. Interferences on ^{202}Pb and ^{205}Pb were monitored by measuring masses 201 and 203 and also by monitoring masses 202 and 205 in unspiked samples. As a result, no corrections were applied. For samples with the ^{202}Pb - ^{205}Pb - ^{233}U - ^{235}U tracer each measured ratio was corrected for fractionation in the data acquisition software using a $^{202}\text{Pb}/^{205}\text{Pb}$ of 0.99989. For single-Pb spike samples, the average fractionation value determined by the ^{202}Pb - ^{205}Pb tracer was used, and this was 0.13 ± 0.04 (2-sigma standard deviation).

On the Triton U was measured in static mode on Faraday cups and 10^{12} ohm resistors as UO_2^+ . Oxygen isotopic composition was monitored by measurement of mass 272 on large U500 loads (Wasserburg et al., 1981). Though the $^{18}\text{O}/^{16}\text{O}$ typically grew from 0.00200 to 0.00208 over the course of an analysis, the most drastic increase occurred at the beginning towards an average value of ~ 0.00205 . As a result, early blocks of data were deleted and the average value was used for all data, and corrected during mass spectrometry. Baselines were measurement at ± 0.5 mass units for 30 seconds every 50 ratios. Correction for mass-fractionation for U was done with the double spike assuming a sample $^{238}\text{U}/^{235}\text{U}$ ratio of 137.88. Measured ratios were reduced using the algorithms of Schmitz and Schoene (2007) and Crowley et al. (2007) (Supplementary Table 1), using the following tracer composition, which has a $^{235}\text{U}/^{205}\text{Pb} = 100.20$ to which a total uncertainty of 0.1 was assigned (Supplementary Table 2).

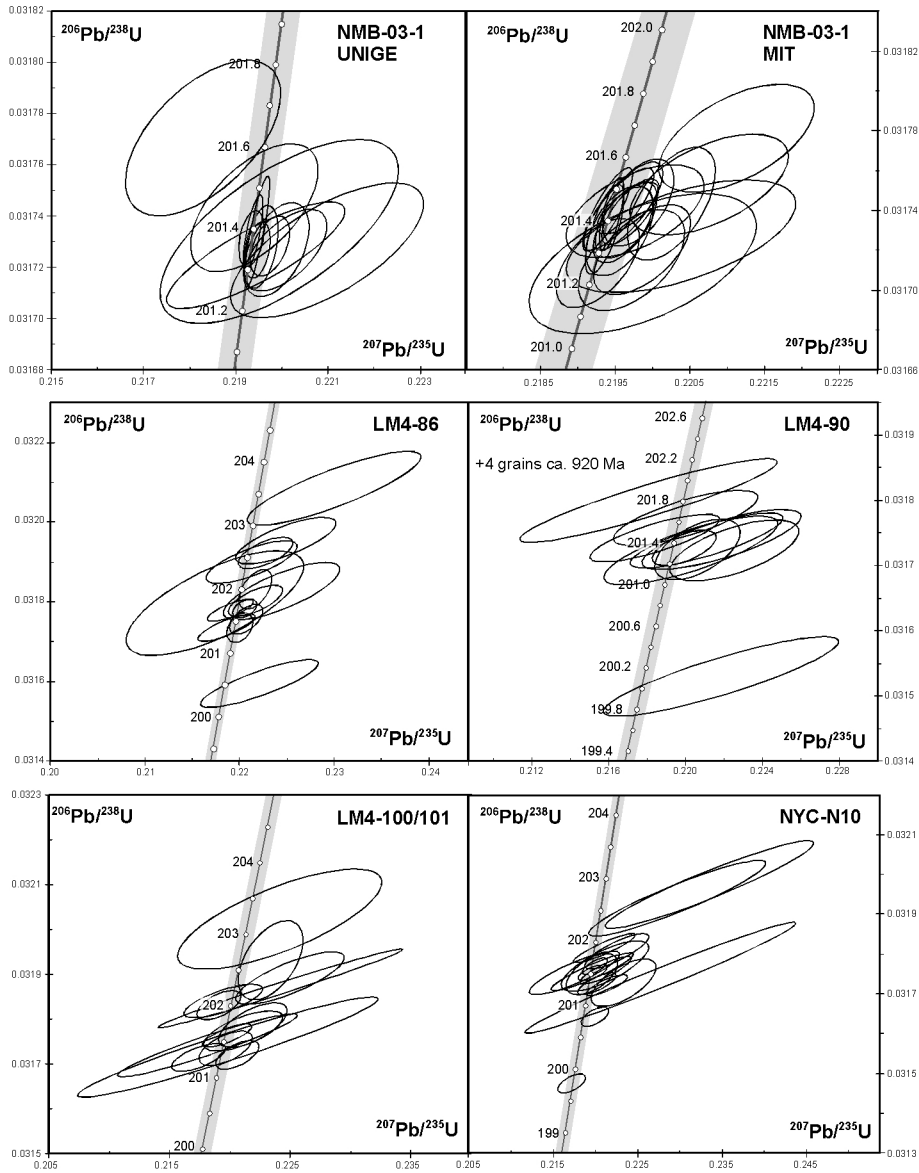
All ashbed zircons were measured at UNIGE. Because many of the tuff zircons in this study are very low-U, the largest uncertainty in the calculated date is that of the correction for common lead. We measured over 40 total procedural blanks at UNIGE

over the course of this study, spiked either the tracer containing ^{202}Pb or with the single Pb tracer. We found that the amount of common Pb in blanks agreed well with that found in zircon analyses, suggesting all common Pb came from blank. The tracer-stripped isotopic composition resulting from each tracer was slightly different, and this is likely due to different isotopic compositions in the tracers themselves. Thus, zircons analyzed with ^{205}Pb - ^{233}U - ^{235}U were reduced using the corresponding blank composition and vice versa. After 2-sigma outlier rejection, the composition of fifteen ^{205}Pb - ^{233}U - ^{235}U -spiked blanks was: $^{206}\text{Pb}/^{204}\text{Pb} = 18.08 \pm 0.66$, $^{207}\text{Pb}/^{204}\text{Pb} = 15.79 \pm 0.45$, $^{208}\text{Pb}/^{204}\text{Pb} = 37.55 \pm 0.93$ (2-sigma standard deviations) and for 27 ^{202}Pb - ^{205}Pb - ^{233}U - ^{235}U -spiked blanks was: $^{206}\text{Pb}/^{204}\text{Pb} = 18.39 \pm 0.22$, $^{207}\text{Pb}/^{204}\text{Pb} = 15.62 \pm 0.20$, $^{208}\text{Pb}/^{204}\text{Pb} = 37.62 \pm 0.78$ (2-sigma standard deviations). To test the accuracy of the ^{202}Pb - ^{205}Pb - ^{233}U - ^{235}U composition, we intentionally picked very small fragments (<20 μm diameter) of North Mtn. Basalt (NMB-03-1) in order to achieve similar ratios of radiogenic Pb to blank Pb as those observed in ash bed zircons. Because this did not introduce scatter into the results, we conclude the blank composition is approximately correct, and not the cause of the range in dates seen in each ash bed. Blank calculation at MIT followed a similar procedure, and resulted in the following composition, used to reduce all NMB-03-1 data: $^{206}\text{Pb}/^{204}\text{Pb} = 18.30 \pm 0.26$, $^{207}\text{Pb}/^{204}\text{Pb} = 15.38 \pm 0.17$, $^{208}\text{Pb}/^{204}\text{Pb} = 37.45 \pm 0.72$.

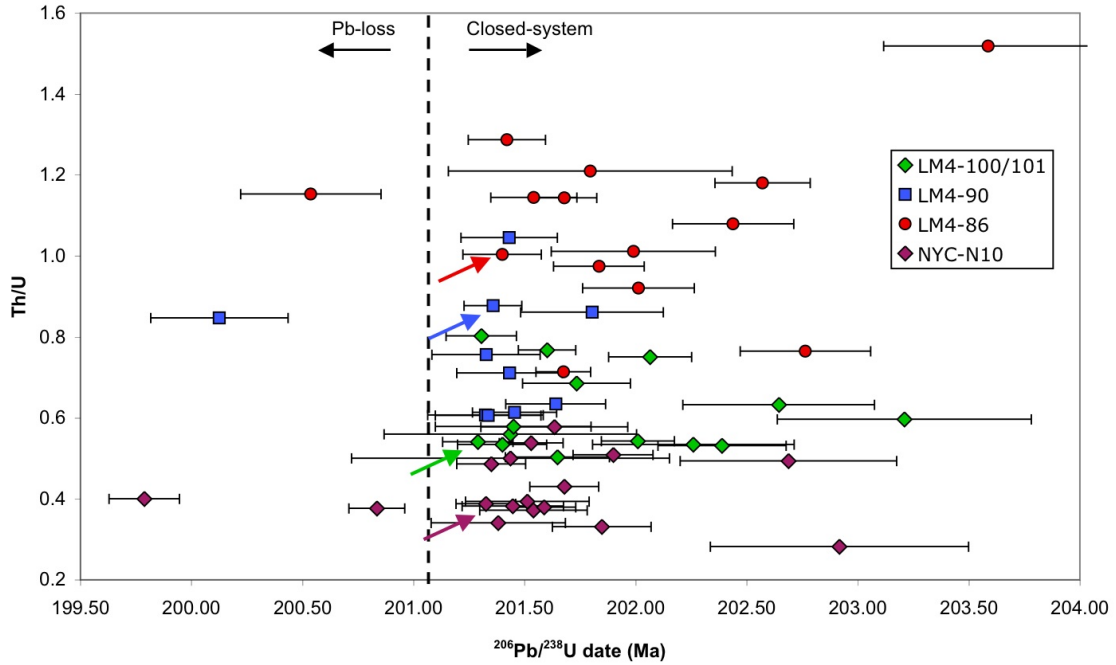
References cited (for Supplementary text)

- Crowley, J.L., Schoene, B., and Bowring, S.A., 2007, U-Pb dating of zircon in the Bishop Tuff at the millennial scale: *Geology*, v. 35, p. 1123-1126; doi: 10.1130/G24017A.
- Gerstenberger, H., and Haase, G., 1997, A highly effective emitter substance for mass spectrometric Pb isotope ratio determinations: *Chemical Geology*, v. 136, p. 309-312.

- Greenough, J.D., and Dostal, J., 1992, Cooling history and differentiation of a thick North Mountain Basalt flow (Nova Scotia, Canada): *Bulletin of Volcanology*, v. 55, p. 63-73.
- Guex, J., Bartolini, A., Atudorei, V., and Taylor, D., 2004, High-resolution ammonite and carbon isotope stratigraphy across the Triassic-Jurassic boundary at New York Canyon (Nevada): *Earth and Planetary Science Letters*, v. 225, p. 29-41.
- Hodych, J.P., and Dunning, G.R., 1992, Did the Manicouagan impact trigger end-of-Triassic mass extinction?: *Geology*, v. 20, p. 21-54.
- Jaffey, A.H., Flynn, K.F., Glendenin, L.E., Bentley, W.C., and Essling, A.M., 1971, Precision measurement of half-lives and specific activities of ^{235}U and ^{238}U : *Physical Review*, v. C4, p. 1889-1906.
- Kontak, D.J., 2008, On the edge of CAMP: Geology and volcanology of the Jurassic North Mountain Basalt, Nova Scotia: *Lithos*, v. 101, p. 74-10; doi:10.1016/j.lithos.2007.07.013.
- Krogh, T.E., 1973, A low contamination method for hydrothermal decomposition of zircon and extraction of U and Pb for isotopic age determination: *Geochimica et Cosmochimica Acta*, v. 37, p. 485-494.
- Schaltegger, U., Guex, J., Bartolini, A., Schoene, B., and Ovtcharova, M., 2008, Precise U-Pb age constraints for end-Triassic mass extinction, its correlation to volcanism and Hettangian post-extinction recovery: *Earth and Planetary Science Letters*, v. 267, p. 266-275, doi:10.1016/j.epsl.2007.11.031.
- Schmitz, M.D., and Schoene, B., 2007, Derivation of isotope ratios, errors, and error correlations for U-Pb geochronology using ^{205}Pb - ^{235}U -(^{233}U)-spike isotope dilution thermal ionization mass spectrometric data: *Geochemistry, Geophysics, Geosystems*, v. 8, p. Q08006, doi: 10.1029/2006GC001492.
- Schoene, B., Crowley, J.L., Condon, D.C., Schmitz, M.D., and Bowring, S.A., 2006, Reassessing the uranium decay constants for geochronology using ID-TIMS U-Pb data: *Geochimica et Cosmochimica Acta*, v. 70, p. 426-445.
- Ward, P.D., Garrison, G.H., Williford, K.H., Kring, D.A., Goodwin, D., Beattie, M.J., and McRoberts, C.A., 2007, The organic carbon isotopic and paleontological record across the Triassic-Jurassic boundary at the candidate GSSP section at Ferguson Hill, Muller Canyon, Nevada, USA: *Palaeogeography, Palaeoclimatology, Palaeoecology*, v. 244, p. 281-289.
- Wasserburg, G.J., Jacouen, S.B., DePaolo, D.J., McCulloch, M.T., and Wen, T., 1981, Precise determinations of Sm/Nd ratios, Sm and Nd isotopic abundances in standard solutions: *Geochimica Cosmochimica Acta*, v. 45, p. 2311-2323.



Supplementary Fig. 1. Concordia plots for samples from this study. Uncertainties are at the 95% confidence level and were calculated using the algorithms in Crowley et al. (2007) and Schmitz and Schoene (2007).



Supplementary Fig. 2: Th/U ratio plotted versus age (Supplementary Table 3) for each single zircon analysis. Th/U from each sample form overlapping clusters, and the average Th/U of zircons from the each Pucara sample decrease with increasing stratigraphic height. The youngest zircon from each sample (indicated by color-coded arrows), chosen as the eruption age, follow this same trend. The overlap in populations may be evidence of zircon inheritance and recycling from older batches of magma or host rocks.

Supplementary Table 1: U-Pb ID-TIMS isotopic data

Sample	tracer	$\frac{Tl}{U}$		$\frac{^{206}Pb}{^{204}Pb}$		$\frac{^{208}Pb}{^{206}Pb}$		$\frac{^{207}Pb}{^{206}Pb}$		Radiogenic Isotope Ratios		Isotopic Ages							
		(c)	(d)	(e)	(f)	(g)	(h)	(i)	(j)	(k)	(l)	(m)	(n)	(o)					
NMB-03-1 (MIT)																			
z48	ETS35	2.855	87	0.46	3232	0.908	0.050145	0.178	0.219272	0.206	0.031714	0.057	0.592	201.74	4.14	201.30	0.38	201.27	0.11
z49	ETS35	1.834	39	0.42	1740	0.585	0.050281	0.525	0.219868	0.567	0.031714	0.092	0.523	208.03	12.18	201.80	1.04	201.27	0.18
z51	ETS35	1.595	58	1.16	2701	0.508	0.050248	0.235	0.219729	0.265	0.031715	0.066	0.544	206.50	5.46	201.68	0.48	201.27	0.13
z44	ETS35	1.475	49	1.17	2354	0.470	0.050261	0.226	0.219825	0.253	0.031721	0.058	0.560	207.06	5.23	201.76	0.46	201.31	0.11
z38	ETS35	1.245	105	1.04	5290	0.396	0.050202	0.108	0.219603	0.146	0.031726	0.070	0.710	204.37	2.51	201.58	0.27	201.34	0.14
z43	ETS35	1.472	23	1.02	1127	0.470	0.050378	0.529	0.220381	0.568	0.031727	0.074	0.571	212.49	12.26	202.23	1.04	201.35	0.15
z68	ETS35	2.161	198	0.50	8240	0.687	0.050147	0.080	0.219395	0.117	0.031730	0.057	0.788	201.83	1.87	201.41	0.21	201.37	0.11
z67	ETS35	1.167	88	0.66	4498	0.371	0.050196	0.137	0.219609	0.168	0.031731	0.061	0.641	204.09	3.17	201.58	0.31	201.37	0.12
z70	ETS35	1.811	237	0.48	10553	0.576	0.050152	0.073	0.219415	0.112	0.031731	0.058	0.814	202.03	1.69	201.42	0.20	201.37	0.12
z36	ETS35	2.084	99	0.43	4183	0.663	0.050193	0.142	0.219632	0.170	0.031736	0.052	0.643	203.95	3.30	201.60	0.31	201.40	0.10
z28	ETS35	2.281	107	0.63	4387	0.726	0.050203	0.129	0.219682	0.157	0.031737	0.050	0.668	204.39	2.99	201.64	0.29	201.41	0.10
z35	ETS35	2.313	42	0.88	1703	0.737	0.050219	0.316	0.219771	0.345	0.031740	0.059	0.552	205.13	7.33	201.72	0.63	201.43	0.12
z52	ETS35	2.086	94	0.43	3976	0.664	0.050171	0.148	0.219565	0.177	0.031740	0.057	0.627	202.90	3.43	201.55	0.32	201.43	0.11
z37	ETS35	2.135	216	0.58	9030	0.679	0.050142	0.077	0.219443	0.113	0.031741	0.054	0.803	201.57	1.78	201.45	0.21	201.44	0.11
z26	ETS35	2.145	112	0.39	4695	0.683	0.050193	0.136	0.219690	0.165	0.031744	0.055	0.648	203.95	3.16	201.65	0.30	201.46	0.11
z29	ETS35	1.888	270	0.32	11823	0.600	0.050169	0.059	0.219584	0.097	0.031744	0.048	0.882	202.83	1.38	201.56	0.18	201.46	0.10
z27	ETS35	2.188	82	0.42	3410	0.698	0.050324	0.190	0.220263	0.222	0.031744	0.075	0.572	209.98	4.39	202.13	0.41	201.46	0.15
z45	ETS35	1.930	81	0.78	3537	0.615	0.050219	0.152	0.219806	0.180	0.031745	0.052	0.627	205.14	3.54	201.75	0.33	201.46	0.10
z42	ETS35	1.862	33	0.74	1474	0.595	0.050413	0.379	0.220719	0.411	0.031754	0.064	0.551	214.08	8.78	202.51	0.75	201.52	0.13
z34	ETS35	2.444	49	0.34	1945	0.782	0.050468	0.349	0.221120	0.381	0.031777	0.069	0.537	216.61	8.08	202.84	0.70	201.66	0.14

NMB-03-1 (UNIGE)

z6	ET2535	1.837	12	2.02	565	0.584	0.050160	0.680	0.219416	0.724	0.031725	0.053	0.828	202.42	15.79	201.42	1.32	201.34	0.11
z3	ET2535	1.853	100	0.92	4446	0.590	0.050171	0.092	0.219473	0.101	0.031727	0.028	0.461	202.92	2.13	201.47	0.18	201.35	0.06
z2	ET2535	1.355	24	0.85	1177	0.432	0.050303	0.324	0.220053	0.347	0.031727	0.041	0.586	209.04	7.52	201.95	0.64	201.35	0.08
z7	ET2535	1.094	10	2.46	519	0.350	0.050505	0.728	0.220935	0.776	0.031727	0.069	0.714	218.30	16.86	202.69	1.43	201.35	0.14
z5	ET2535	1.989	43	0.62	1896	0.634	0.050267	0.241	0.219899	0.260	0.031727	0.047	0.479	207.37	5.59	201.83	0.48	201.35	0.09
z11	ET2535	2.498	83	0.32	3276	0.795	0.050182	0.132	0.219532	0.146	0.031728	0.042	0.463	203.44	3.07	201.52	0.27	201.36	0.08
z4	ET2535	1.920	64	1.30	2806	0.612	0.050230	0.143	0.219744	0.154	0.031728	0.030	0.472	205.66	3.31	201.70	0.28	201.36	0.06
z1	ET2535	2.011	219	0.85	9473	0.640	0.050145	0.043	0.219392	0.053	0.031731	0.027	0.588	201.73	1.01	201.40	0.10	201.38	0.05
z10	ET2535	1.978	106	1.18	4609	0.629	0.050129	0.080	0.219321	0.089	0.031732	0.027	0.469	200.96	1.85	201.34	0.16	201.38	0.05
z9	ET2535	2.012	181	0.97	7799	0.640	0.050146	0.056	0.219400	0.075	0.031732	0.046	0.666	201.79	1.30	201.41	0.14	201.38	0.09
z16	ET2535	2.636	12	0.54	483	0.840	0.050268	0.895	0.219948	0.955	0.031734	0.093	0.667	207.42	20.77	201.87	1.75	201.39	0.18
z12	ET2535	1.998	258	0.46	11145	0.636	0.050168	0.039	0.219575	0.052	0.031743	0.033	0.680	202.79	0.89	201.56	0.10	201.45	0.07
z15	ET2535	2.273	20	0.70	842	0.722	0.050124	0.487	0.219387	0.521	0.031744	0.064	0.567	200.77	11.31	201.40	0.95	201.45	0.13
z17	ET2535	3.096	19	0.57	689	0.979	0.049835	0.589	0.218309	0.630	0.031771	0.079	0.562	187.32	13.71	200.50	1.15	201.62	0.16

LM4-86 (UNIGE)

z27	ET2535	1.153	4	0.74	212	0.373	0.050984	2.144	0.222118	2.281	0.031597	0.160	0.862	240.10	49.4	203.67	4.21	200.54	0.32
z26	ET2535	1.004	7	0.56	381	0.318	0.049973	1.053	0.218663	1.121	0.031735	0.089	0.773	193.73	24.5	200.80	2.04	201.40	0.18
z12	ET535	1.287	18	0.69	937	0.410	0.050285	0.493	0.220052	0.536	0.031739	0.088	0.552	208.18	11.4	201.95	0.98	201.42	0.17
z10	ET535	1.145	13	1.41	701	0.366	0.050389	0.597	0.220641	0.647	0.031758	0.098	0.560	212.95	13.8	202.44	1.19	201.54	0.19
z23	ET2535	0.714	15	0.71	888	0.228	0.050330	0.459	0.220532	0.491	0.031779	0.062	0.559	210.25	10.6	202.35	0.90	201.67	0.12
z28	ET2535	1.143	9	0.76	468	0.363	0.049993	0.844	0.219062	0.899	0.031780	0.074	0.751	194.69	19.6	201.13	1.64	201.68	0.15
z16	ET535	1.210	2	1.07	139	0.381	0.049563	3.394	0.217306	3.611	0.031799	0.321	0.698	174.57	79.2	199.67	6.54	201.80	0.64
z24	ET2535	0.975	7	0.68	405	0.312	0.050544	0.993	0.221650	1.059	0.031805	0.103	0.671	220.10	23.0	203.28	1.95	201.83	0.20
z19	ET2535	1.012	4	0.55	214	0.327	0.051138	2.104	0.224428	2.240	0.031830	0.186	0.750	247.05	48.4	205.59	4.17	201.99	0.37
z11	ET535	0.921	13	1.28	726	0.295	0.050489	0.593	0.221604	0.647	0.031833	0.126	0.508	217.55	13.7	203.24	1.19	202.01	0.25
z20	ET2535	1.079	4	1.10	242	0.344	0.050324	1.663	0.221354	1.769	0.031902	0.137	0.793	209.98	38.5	203.04	3.26	202.44	0.27
z17	ET535	1.180	14	0.41	755	0.378	0.050608	0.954	0.222751	1.022	0.031923	0.107	0.660	223.01	22.1	204.20	1.89	202.57	0.21
z22	ET2535	0.765	4	1.16	222	0.247	0.051050	1.796	0.224916	1.912	0.031954	0.147	0.808	243.10	41.4	205.99	3.57	202.76	0.29
z25	ET2535	1.519	3	0.96	140	0.498	0.051952	3.011	0.229830	3.209	0.032085	0.234	0.852	283.28	68.9	210.06	6.09	203.59	0.47

LM4-90 (UNIGE)

z12	ET2535	0.847	4	0.58	229	0.274	0.051021	2.138	0.221818	2.274	0.031531	0.157	0.876	241.80	49.3	203.42	4.19	200.13	0.31
z11	ET2535	0.607	4	0.80	265	0.194	0.050350	1.568	0.220230	1.669	0.031723	0.131	0.780	211.18	36.3	202.10	3.06	201.32	0.26
z4	ET2535	0.757	6	0.75	339	0.244	0.050870	1.146	0.2222507	1.222	0.031724	0.123	0.653	234.93	26.4	203.99	2.26	201.33	0.24
z10	ET2535	0.607	10	0.40	626	0.194	0.050439	0.747	0.220632	0.801	0.031725	0.120	0.514	215.26	17.3	202.44	1.47	201.34	0.24
z8	ET2535	0.877	13	0.62	717	0.280	0.050273	0.581	0.219933	0.620	0.031729	0.066	0.623	207.65	13.5	201.85	1.14	201.36	0.13
z3	ET2535	1.045	5	1.19	296	0.335	0.050511	1.380	0.221052	1.468	0.031740	0.110	0.818	218.56	31.9	202.78	2.70	201.43	0.22
z2	ET2535	0.711	5	1.46	290	0.228	0.050699	1.434	0.221880	1.527	0.031740	0.120	0.789	227.19	33.1	203.47	2.81	201.43	0.24
z15	ET2535	0.614	6	0.70	385	0.194	0.049905	1.212	0.218426	1.288	0.031744	0.095	0.814	190.55	28.2	200.60	2.34	201.45	0.19
z13	ET2535	0.635	6	0.61	371	0.202	0.050234	1.323	0.220074	1.408	0.031774	0.113	0.765	205.84	30.7	201.97	2.58	201.64	0.23
z1	ET2535	0.862	3	1.80	176	0.272	0.049729	2.385	0.218042	2.533	0.031800	0.162	0.920	182.37	55.6	200.28	4.60	201.80	0.32
z14	ET2535	0.522	17	0.62	998	0.160	0.069613	0.308	1.469497	0.415	0.153101	0.247	0.676	916.96	6.3	917.92	2.51	918.32	2.11
z5	ET2535	0.566	9	0.63	573	0.174	0.070359	0.539	1.486947	0.597	0.153277	0.116	0.570	938.84	11.0	925.07	3.62	919.31	0.99
z9	ET2535	0.502	49	0.42	2906	0.154	0.070008	0.100	1.487183	0.117	0.154069	0.041	0.540	928.60	2.1	925.17	0.71	923.73	0.36
z7	ET2535	0.473	13	0.81	809	0.145	0.070208	0.342	1.496745	0.478	0.154619	0.302	0.700	934.43	7.0	929.06	2.91	926.80	2.61

LM4-100/101 (UNIGE)

z16	ET2535	0.541	8	0.66	477	0.171	0.049735	0.842	0.217501	0.897	0.031718	0.080	0.704	182.62	19.6	199.83	1.63	201.29	0.16
z7	ET2535	0.803	13	0.53	770	0.257	0.050446	0.638	0.220630	0.681	0.031720	0.080	0.583	215.61	14.8	202.43	1.25	201.30	0.16
z12	ET2535	0.535	9	0.81	562	0.170	0.050194	0.768	0.219630	0.821	0.031735	0.101	0.567	203.98	17.8	201.60	1.50	201.40	0.20
z17	ET2535	0.560	1	2.18	102	0.178	0.050238	4.363	0.219865	4.638	0.031741	0.287	0.959	206.03	101.2	201.80	8.49	201.44	0.57
z9	ET2535	0.578	2	1.01	166	0.183	0.049842	2.665	0.218144	2.832	0.031743	0.177	0.945	187.61	62.0	200.36	5.15	201.45	0.35
z13	ET2535	0.768	9	0.96	538	0.244	0.050170	0.733	0.219749	0.780	0.031768	0.065	0.746	202.87	17.0	201.70	1.43	201.60	0.13
z15	ET2535	0.503	6	0.45	379	0.161	0.050470	1.129	0.221116	1.203	0.031775	0.118	0.663	216.70	26.1	202.84	2.21	201.65	0.23
z4	ET2535	0.686	7	0.61	423	0.220	0.050626	1.003	0.221898	1.076	0.031789	0.122	0.634	223.86	23.2	203.49	1.98	201.73	0.24
z18	ET2535	0.543	10	0.57	618	0.172	0.049919	0.639	0.219100	0.683	0.031833	0.083	0.571	191.21	14.9	201.16	1.25	202.01	0.16
z8	ET2535	0.751	7	0.51	402	0.238	0.049982	1.144	0.219440	1.217	0.031842	0.094	0.792	194.17	26.6	201.44	2.22	202.07	0.19
z10	ET2535	0.534	2	2.60	118	0.173	0.051022	3.514	0.224223	3.738	0.031873	0.228	0.986	241.82	81.0	205.42	6.95	202.26	0.45
z3	ET2535	0.531	4	0.94	262	0.172	0.051169	1.518	0.225014	1.622	0.031894	0.145	0.743	248.44	34.9	206.07	3.03	202.39	0.29
z1	ET2535	0.633	9	1.05	568	0.203	0.050732	0.948	0.223381	1.033	0.031934	0.217	0.479	228.68	21.9	204.72	1.91	202.64	0.43
z5	ET2535	0.597	2	2.00	149	0.192	0.050743	2.913	0.224059	3.105	0.032025	0.286	0.699	229.15	67.3	205.28	5.77	203.21	0.57

NYC-N10 (UNIGE)

z15	ET2535	0.400	12	0.51	761	0.127	0.050033	0.543	0.217149	0.582	0.031477	0.081	0.533	196.55	12.6	199.53	1.05	199.79	0.16
z7	ET2535	0.377	10	1.10	649	0.120	0.050387	0.597	0.219848	0.637	0.031645	0.064	0.657	212.88	13.8	201.78	1.17	200.83	0.13
z12	ET2535	0.388	7	1.15	447	0.125	0.050639	0.848	0.221498	0.903	0.031723	0.068	0.822	224.44	19.6	203.16	1.66	201.33	0.13
z16	ET2535	0.486	8	0.64	498	0.155	0.050322	0.809	0.220136	0.862	0.031727	0.078	0.706	209.89	18.7	202.02	1.58	201.35	0.15
z10	ET2535	0.341	5	0.53	331	0.110	0.051045	1.303	0.223335	1.392	0.031732	0.153	0.620	242.87	30.0	204.68	2.58	201.38	0.30
z3	ET2535	0.500	1	3.33	82	0.165	0.052044	5.383	0.227771	5.737	0.031741	0.361	0.982	287.37	123.0	208.36	10.81	201.44	0.72
z6	ET2535	0.383	11	0.61	690	0.121	0.049967	0.692	0.218690	0.743	0.031743	0.115	0.503	193.46	16.1	200.82	1.35	201.45	0.23
z5	ET2535	0.393	3	1.30	217	0.124	0.049684	1.912	0.217521	2.032	0.031753	0.140	0.870	180.22	44.5	199.84	3.69	201.51	0.28
z18	ET2535	0.539	11	0.43	669	0.171	0.050187	0.604	0.219746	0.645	0.031756	0.073	0.604	203.67	14.0	201.70	1.18	201.53	0.14
z1	ET2535	0.372	4	1.09	242	0.118	0.050170	1.727	0.219680	1.837	0.031758	0.122	0.907	202.86	40.1	201.64	3.36	201.54	0.24
z9	ET2535	0.379	7	0.52	484	0.121	0.050340	0.801	0.220478	0.854	0.031765	0.072	0.745	210.71	18.6	202.31	1.57	201.59	0.14
z4	ET2535	0.578	4	1.04	245	0.185	0.050495	1.858	0.221208	1.979	0.031773	0.167	0.746	217.82	43.0	202.91	3.64	201.63	0.33
z17	ET2535	0.431	11	0.49	711	0.137	0.050206	0.591	0.219992	0.632	0.031780	0.078	0.570	204.54	13.7	201.90	1.16	201.68	0.15
z13	ET2535	0.331	5	0.92	302	0.106	0.050724	1.373	0.222453	1.462	0.031807	0.112	0.812	228.31	31.7	203.95	2.70	201.85	0.22
z2	ET2535	0.509	5	1.12	309	0.163	0.050405	1.260	0.221110	1.341	0.031815	0.091	0.898	213.71	29.2	202.83	2.46	201.90	0.18
z8	ET2535	0.494	2	0.88	119	0.163	0.052173	3.514	0.229776	3.744	0.031942	0.244	0.945	293.01	80.2	210.01	7.10	202.69	0.49
z14	ET2535	0.282	1	1.04	112	0.094	0.053028	4.072	0.233811	4.342	0.031978	0.291	0.932	330.02	92.4	213.34	8.36	202.92	0.58

(a) z1, z2 etc. are labels for fractions composed of single zircon grains or fragments; all fractions annealed and chemically abraded after Mattinson (2005).

(b) EARTHTIME tracer used. ET535 = 205Pb-233U-235U, ET2535 = 202Pb-205Pb-233U-235U

(c) Model Th/U ratio calculated from radiogenic 208Pb/206Pb ratio and 206Pb/238U age.

(d) Pb* and Pb_c represent radiogenic and common Pb, respectively; mol % ²⁰⁶Pb* with respect to blank Pb.

(e) Measured ratio corrected for spike and fractionation only. Mass fractionation correction of 0.25 ± 0.02 (1-sigma) %/amu (atomic mass unit) was applied to MIT North Mtn. Basalt analyses.

UNIGE data corrected using either the double-Pb tracer or with 0.13±0.02 %/amu.

(f) Corrected for fractionation, spike, and common Pb; all common Pb was assumed to be procedural blank: 206Pb/204Pb = 18.39 ± 0.91%; 207Pb/204Pb = 15.45 ± 0.66%; 208Pb/204Pb = 37.62 ± 0.78% (all uncertainties 1-sigma). 206Pb/238U and 207Pb/206Pb ratios corrected for initial disequilibrium in 230Th/238U using Th/U [magma] = 4 ± 1 (1-sigma).

(g) Errors are 2-sigma, propagated using the algorithms of Schmitz and Schoene (2007) and Crowley et al. (2007).

(h) Calculations are based on the decay constants of Jaffey et al. (1971).

Supplementary Table 2: composition of the EARTHTIME U-Pb tracer used in this study

205Pb	9.882260145E-12		[mol/g]
235U	9.902024666E-10		[mol/g]
235U/205Pb	100.20	0.05	± 1σ [%]
202Pb/205Pb	9.998900000E-01	± 0.005	± 1σ [%]
206Pb/205Pb	2.989385290E-04	± 0.74	± 1σ [%]
207Pb/205Pb	2.407104342E-04	± 0.10	± 1σ [%]
204Pb/205Pb	8.875074984E-05	± 0.10	± 1σ [%]
208Pb/205Pb	5.917328387E-04	± 0.10	± 1σ [%]
207Pb/206Pb	8.052171630E-01	± 0.10	± 1σ [%]
204Pb/206Pb	2.970280430E-01	± 0.10	± 1σ [%]
238U/235U	3.087000000E-03	± 0.005	± 1σ [%]
233U/235U	9.946400000E-01	± 0.005	± 1σ [%]
238U/233U	3.103635486E-03	± 0.005	± 1σ [%]

<u>Eruption Ages</u>	N	date	±	N (MSWD)	date	±	N (MSWD)	date	±
NMB UNIGE	1	201.34	0.11	13 (0.8)	201.37	0.02			
NMB MIT	1	201.27	0.11	19 (1.4)	201.39	0.03			
LM4-86	1	201.40	0.18	3 (0.7)	201.45	0.10	4 (3.1)	201.54	0.22
LM4-90	1	201.36	0.13	4 (0.0)	201.35	0.09	8 (0.9)	201.41	0.07
LM4-100/101	1	201.29	0.16	3 (0.4)	201.32	0.10	5 (0.3)	201.33	0.09
NYC-N10	1	201.33	0.13	3 (0.1)	201.34	0.09	10 (1.3)	201.46	0.08
<u>Timing of Events</u>									
age of TJB		201.31	0.18		201.33	0.11		201.36	0.12
duration of $\delta^{13}\text{C}$ excursion		0.07	+0.22/ -0.07		0.11	+0.13/ -0.11		0.08	+0.23/ -0.08

Supplementary Table 3. Estimates for eruption ages of samples from this study using different interpretations of the data. All dates are $^{206}\text{Pb}/^{238}\text{U}$ dates in millions of years. All uncertainties are at the 95% confidence interval. N = number of data points used in calculation, beginning with the youngest closed-system zircon (Fig 1C) and including the next oldest; MSWD = mean square of weighted deviates for weighted-means with $N > 2$. Ages for events are calculated as follows: age of Triassic-Jurassic Boundary (TJB) = maximum limits of LM4-90 and minimum limits of LM4-100/101; duration of $\delta^{13}\text{C}$ excursion = age of LM4-86 - age of NYC-N10, uncertainties calculated using standard error-propagation, assuming duration cannot be < 0 .